Mechanical Systems and Signal Processing 132 (2019) 595–608

Contents lists available at ScienceDirect

Mechanical Systems and Signal Processing

journal homepage: www.elsevier.com/locate/ymssp

On the modelling of membrane-coupled Helmholtz resonator and its application in acoustic metamaterial system

Guobiao Hu [a], Lihua Tang [a,*], Xiaobin Cui [b,a]

[a] Department of Mechanical Engineering, University of Auckland, Auckland 1010, New Zealand
[b] Department of Applied Physics, Nanjing Tech University, Nanjing 211816, China

ARTICLE INFO

Article history:
Received 26 March 2019
Received in revised form 4 June 2019
Accepted 10 July 2019

Keywords:
Helmholtz resonator
Membrane
Acoustic metamaterial
Acoustic-mechanical interaction

ABSTRACT

In recent years, the Helmholtz resonator and membrane are two popular elements that have been vastly employed in the design of energy harvesters and metamaterials. In this paper, a theoretical study of the modelling of the membrane-coupled Helmholtz resonator is presented. The membrane is first represented with lumped parameters as a single-degree-of-freedom piston/centre-mass model. The physical meaning of the effective force-bearing area is explained. The membrane-coupled Helmholtz resonator is then modelled as a multiple-degree-of-freedom system. From the acoustic-mechanical interaction perspective, transformation coefficients are derived to bridge the acoustic and mechanical domains. Inspired by the fact that the membrane-coupled Helmholtz resonator exhibits multiple resonances in the low frequency regime, an acoustic metamaterial system is proposed by integrating the membrane-coupled Helmholtz resonators. A theoretical model of the proposed acoustic metamaterial is developed and multiple band gaps are predicted from the band structure analysis. All the theoretical models presented in this paper have been verified by corresponding finite element models.

1. Introduction

The Helmholtz resonator is a very classic acoustic system that has been extensively studied decades ago [1,2]. In recent years, with the flourishing development on the research of energy harvesting and metamaterials, Helmholtz resonators are being vastly used in the design of acoustic energy harvesters [3–6] for sound augmentation and acoustic metamaterials [7–11] for noise attenuation. Horowitz et al. [3] proposed an acoustic energy harvester consisting of a Helmholtz resonator whose bottom was a circular diaphragm integrated with a piezoelectric ring. The entire system was represented by an equivalent circuit model with three degrees of freedom. From the simulated results, two resonant peaks were observed. A similar multiple-degree-of-freedom Helmholtz resonator model was studied by Liu et al. [12]. They presented a more detailed modelling procedure of the acoustic-mechanical system with lumped parameters. Afterwards, they employed that model for acoustic energy harvesting [13]. Yang et al. [4] designed a Helmholtz resonator with a compliant top plate onto which two piezoelectric beams were bonded. The experimental study showed that the proposed system could achieve an enhanced broadband energy harvesting ability. Matova et al. [14] placed a piezoelectric energy harvester inside of a Helmholtz resonator for harvesting energy from airflow. Their experimental results revealed that a Helmholtz resonator with a membrane bottom could achieve a better performance than that with a rigid bottom. Peng et al. [15] presented an acoustic energy

* Corresponding author.
E-mail address: l.tang@auckland.ac.nz (L. Tang).

https://doi.org/10.1016/j.ymssp.2019.07.017
0888-3270/

harvester with a dual Helmholtz resonator architecture. The proposed system possessed three degrees of freedom and three peaks were captured in the voltage frequency responses. More related work on the use of Helmholtz resonators and/or membranes for energy harvesting can be referred to [5,16–19].

Regarding the application of Helmholtz resonator in the design of metamaterials, Fang et al. [7] presented an early study of an acoustic metamaterial consisting of an array of subwavelength Helmholtz resonators. Their experimental results matched well with the theoretical calculation based on the homogenized-media theory. For the same model, Wang et al. [9] presented a systematic theoretical study. By using the interface response theory, they calculated the band structures, transmission spectra, and defect states of such kind of metamaterial. Li et al. [8] proposed an acoustic metamaterial with a coupled Helmholtz resonator configuration. They achieved near-total absorption at the central frequency. Other related studies on the similar metamaterial model can be referred to [10,11].

In recent years, membrane-type acoustic metamaterials have also attracted lots of research interests [20–22], since they can achieve acoustic attenuation at a deep sub-wavelength scale. Yang et al. [22] proposed an acoustic metamaterial comprising two coupled membranes. It was proved that the proposed metamaterial could exhibit broadband double negativity. Li et al. [23] designed a membrane-type metamaterial that was capable of both sound insulation and energy harvesting. Gao et al. [24] studied a membrane acoustic metamaterial, wherein the membrane was attached with an annular rigid ring. The low frequency band gap behaviour in the proposed metamaterial was observed and the sound transmission loss of the system was investigated.

From the literature review, it can be found that both Helmholtz resonator and membrane are two popular elements that have been widely employed in the design of energy harvesting systems and metamaterials in recent years. Moreover, several recent literature proposed and explored the idea of using membrane to design controllable/adaptive Helmholtz resonators [25–27]. Though vast efforts for modelling of Helmholtz resonators and membranes have been reported, there lacks a systematic study on the modelling of the coupled system combining them and being integrated into acoustic metamaterials. In this paper, we start from the modelling of the membrane. For simplifying the modelling process, two single-degree-of-freedom (SDOF) models, i.e., piston model and centre-mass model, are proposed to predict the dynamic behaviour of the membrane. The equivalent lumped parameters of the two SDOF models are analytically derived. The significance of distinguishing the effective force-bearing area and the actual membrane area is discussed in details. The accuracy of the proposed models is verified by the finite element analysis (FEA). Subsequently, the membrane is combined with the Helmholtz resonator to form an acoustic-mechanical coupled multiple-degree-of-freedom (MDOF) system. The acoustic-mechanical coupling issue is addressed to bridge the two domains. The transformation coefficients are derived for the cases when the membrane is represented by the piston model and the centre-mass model, respectively. The developed MDOF model is then verified by FEA. Finally, an acoustic metamaterial system integrated with the membrane-coupled Helmholtz resonator is proposed. On the basis of the derived MDOF models for the membrane-coupled Helmholtz resonator, the theoretical model for the proposed acoustic metamaterial system is developed. The band structure analysis based on the theoretical model is also confirmed by FEA.

2. SDOF representation for membrane

2.1. Distributed parameter model

Fig. 1 shows the schematic of a circular membrane of radius a, uniform areal density ρ_a and tension T_s. A polar coordinate system with the origin at the circular membrane centre is utilized to define the spatial location of the membrane.

The governing equation of motion of the circular membrane under forced axisymmetric vibration is expressed as [28]:

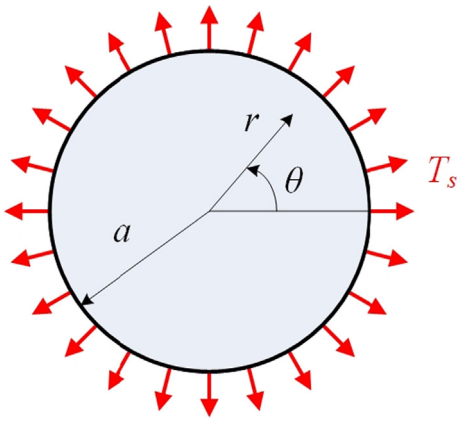

Fig. 1. A circular membrane in polar coordinate system.

$$\frac{\partial^2 w(r,t)}{\partial r^2}+\frac{1}{r}\frac{\partial w(r,t)}{\partial r}-\frac{1}{c^2}\frac{\partial^2 w(r,t)}{\partial t^2}-\frac{c_d}{T_s}\frac{\partial w(r,t)}{\partial t}=\frac{-p_a}{\rho_a c^2} \tag{1}$$

where $w(r,t)$ describes the deflection of the membrane as a function of the radial position r and time t, $c=\sqrt{T_s/\rho_a}$, p_a is the uniform pressure distributed over the surface of the membrane, c_d is viscous damping coefficient. Assuming a harmonic pressure excitation $p_a=P_a e^{j\omega t}$ ($j=\sqrt{-1}$) in which P_a is the amplitude of the pressure and using the modal superposition method, the steady-state solution of the membrane deflection $w(r,t)$ is assumed to be in the form as:

$$w(r,t)=\sum_{n=1}^{\infty}\phi_n(r)\eta_n(t) \tag{2}$$

where $\eta_n(t)$ is the modal coordinate, $\phi_n(r)$ is the mode shape with the solution as:

$$\phi_n(r)=AJ_0(k_n r) \tag{3}$$

where A is an arbitrary constant, $J_0(x)$ is the Bessel function of the first kind of order 0,$k_n=\omega_n/c$ and ω_n is the natural frequency of the nth mode of the membrane. Since under the uniform pressure excitation, non-axisymmetric vibration motion of the membrane can not be excited, only axisymmetric vibration modes of the membrane are considered and the "nth mode" refers to the "nth axisymmetric mode" for short throughout the paper. Substituting Eq. (2) into Eq. (1), multiplying by the mode shapes $\phi_n(r)$, integrating over the radius (i.e., from 0 to a), and then using the orthogonality relations, the modal governing equation can be obtained:

$$\frac{d^2\eta_n(t)}{dt^2}+2\zeta_n\omega_n\frac{d\eta_n(t)}{dt}+\omega_n^2\eta_n(t)=\frac{P_a e^{j\omega t}}{\rho_a}\int_0^a r\phi_n(r)dr \tag{4}$$

where $\zeta_n=c_d/2\rho_a\omega_n$. The modal response can then be obtained as:

$$\eta_n(t)=\frac{\frac{P_a}{\rho_a}\int_0^a r\phi_n(r)dr}{\omega_n^2-\omega^2+j2\zeta_n\omega_n\omega}e^{j\omega t} \tag{5}$$

The displacement corresponds to the nth mode is:

$$w_n(r,t)=\phi_n(r)\eta_n(t) \tag{6}$$

The displacement response of the membrane at an arbitrary position r from the centre is thus:

$$w(r,t)=\sum_{n=1}^{\infty}\phi_n(r)\frac{\frac{P_a}{\rho_a}\int_0^a r\phi_n(r)dr}{\omega_n^2-\omega^2+j2\zeta_n\omega_n\omega}e^{j\omega t} \tag{7}$$

2.2. SDOF model

To represent the membrane as a SDOF model around the nth mode, the kinetic energy of an infinitesimal annular element corresponding to the displacement in the nth mode is:

$$dE_{kn}=\frac{1}{2}(2\pi\rho_a r dr)\left(\frac{\partial w_n(r,t)}{\partial t}\right)^2 \tag{8}$$

where $w_n(r,t)=\phi_n(r)\eta_n(t)$ can be expressed in the following form

$$w_n(r,t)=A_n J_0\left(\frac{\mu_n}{a}r\right)\cos(\omega_n t) \tag{9}$$

where μ_n is the nth root to $J_0(\mu)=0$. The average kinetic energy over a period T of the infinitesimal annular element equals:

$$\overline{dE_{kn}}=\frac{1}{T}\int_0^T\pi\rho_a\left(\frac{\partial w_n(r,t)}{\partial t}\right)^2 r dr dt=\frac{1}{2}\pi\rho_a\omega_n^2A_n^2J_0^2\left(\frac{\mu_n}{a}r\right)rdr \tag{10}$$

Integrating over the radial direction from 0 to a yields the total kinetic energy of the entire membrane averaged over a period:

$$\left(\overline{E_{kn}}\right)_{membrane}=\int\overline{dE_{kn}}=\frac{1}{4}\pi a^2\rho_a\omega_n^2A_n^2J_1^2(\mu_n) \tag{11}$$

2.2.1. Piston model

In the first case, the membrane deformation is treated as a piston model, as shown in Fig. 2(a) and (b). To ensure that the volume displacements of the membrane and equivalent piston are the same, the space-averaged deflection is taken as the displacement of the piston:

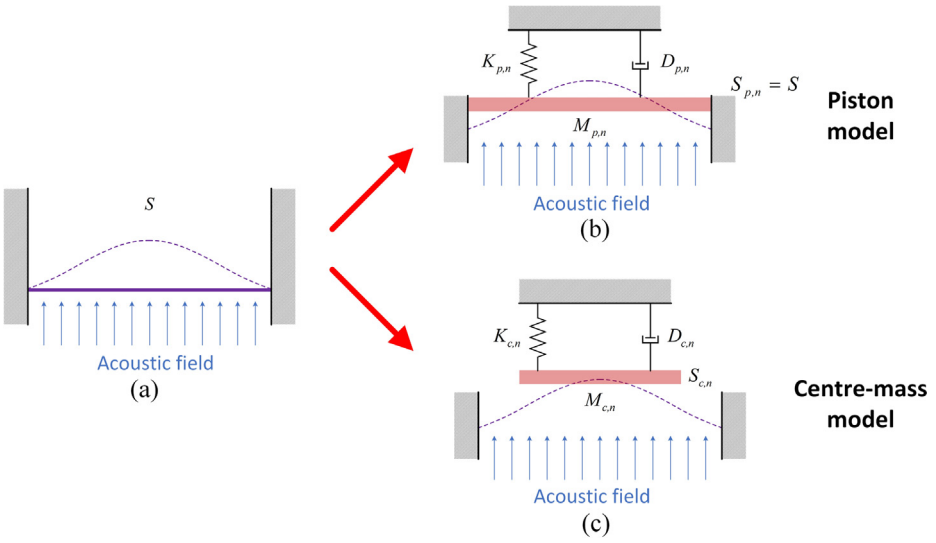

Fig. 2. Schematics of (a) membrane deformation, (b) equivalent SDOF piston model, (c) equivalent SDOF centre-mass model.

$$\langle w_n(t)\rangle = \frac{1}{\pi a^2}\int_0^a 2\pi r w_n(r,t)dr = \frac{2}{\mu_n}A_n J_1(\mu_n)\cos(\omega_n t) \tag{12}$$

The kinetic energy of the piston averaged over a period is:

$$\left(\overline{E_{kn}}\right)_p = \frac{1}{T}\int_0^T \frac{M_{p,n}}{2}\left(\frac{d\langle w_n(t)\rangle}{dt}\right)^2 dt = \frac{M_{p,n}}{\mu_n^2}A_n^2\omega_n^2 J_1^2(\mu_n) \tag{13}$$

where, $M_{p,n}$ is the equivalent mass of the piston, which can be derived by equating Eq. (11) and Eq. (13):

$$M_{p,n} = \frac{\mu_n^2}{4}\pi a^2 \rho_a \tag{14}$$

The equivalent stiffness and the damping coefficient are $K_{p,n} = M_{p,n}\omega_n^2$ and $D_{p,n} = 2\zeta_n M_{p,n}\omega_n^2$, respectively. The equation of motion for the piston model can then be expressed as:

$$M_{p,n}\ddot{y}_n(t) + D_{p,n}\dot{y}_n(t) + K_{p,n}y_n(t) = S_{p,n}p_a(t) \tag{15}$$

where $y_n(t) = \langle w_n(t)\rangle$. Note that the relationship between $y_n(t)$ and the displacement at the centre of the membrane $w_n(0,t)$ can be derived by using Eqs. (9) and (12) as:

$$\frac{y_n(t)}{w_n(0,t)} = \frac{2J_1(\mu_n)}{\mu_n J_0(0)} = \beta_n \tag{16}$$

$S_{p,n}$ is an undetermined parameter whose physical meaning is the effective force-bearing area, i.e., multiplying $p_a(t)$ by $S_{p,n}$ should give the effective force exerted onto the piston. From Eq. (15), one could derive the displacement response solution of the piston:

$$y_n(t) = \frac{S_{p,n}P_a}{M_{p,n}(\omega_n^2 - \omega^2 + j2\zeta_n\omega_n\omega)}e^{j\omega t} \tag{17}$$

$S_{p,n}$ could be determined through the comparison between Eq. (17) and the nth mode component of Eq. (7):

$$S_{p,n} = M_{p,n}\frac{2J_1(\mu_n)}{\mu_n J_0(0)}\frac{\phi_n(0)\int_0^a r\phi_n(r)dr}{\rho_a} \tag{18}$$

By inserting Eqs. (3) and (14) into Eq. (18), interestingly, it is found $S_{p,n} = S = \pi a^2$, which implies that the effective force-bearing area of the piston model is just the membrane area.

2.2.2. Centre-mass model

In the second case, we assume that the equivalent lumped parameters are concentrated at the membrane centre, as shown in Fig. 2(c). Since the equivalent lumped mass is presumed to be at the membrane centre, its velocity, by differentiating Eq. (9) and letting $r = 0$ is:

$$\left.\frac{dw_n(r,t)}{dt}\right|_{r=0} = -A_n\omega_n J_0(0)\sin(\omega_n t) \tag{19}$$

The kinetic energy of the equivalent lumped mass averaged over a period is:

$$\left(\overline{E_{kn}}\right)_c = \frac{1}{T}\int_0^T \frac{M_{c,n}}{2}\left(\left.\frac{dw_n(r,t)}{dt}\right|_{r=0}\right)^2 dt = \frac{1}{4}M_{c,n}\omega_n^2 A_n^2 \tag{20}$$

where, $M_{c,n}$ is The equivalent mass of the centre mass, which can be obtained by equating Eqs. (11) and (20).

$$M_{c,n} = \pi a^2 \rho_a J_1^2(\mu_n) \tag{21}$$

The equivalent stiffness and damping coefficient are $K_{c,n} = M_{c,n}\omega_n^2$ and $D_{c,n} = 2\zeta_n M_{c,n}\omega_n^2$, respectively. The governing equation of the centre-mass model is written as:

$$M_{c,n}\ddot{u}_n(t) + D_{c,n}\dot{u}_n(t) + K_{c,n}u_n(t) = S_{c,n}p_a(t) \tag{22}$$

where $u_n(t) = w_n(0,t)$ is used to denote the displacement in the nth mode of the membrane centre for conciseness, $S_{c,n}$ is an undetermined parameter whose physical meaning is the effective force-bearing area for the nth mode of the membrane, i.e., multiplying $p_a(t)$ by should give the effective force exerted onto the equivalent mass at the membrane centre. From the Eq. (22), one obtains the displacement response of the equivalent lumped centre-mass:

$$u_n(t) = \frac{S_{c,n}P_a}{M_{c,n}\left(\omega_n^2 - \omega^2 + j2\zeta_n\omega_n\omega\right)}e^{j\omega t} \tag{23}$$

By comparing Eq. (23) with the nth mode component of Eq. (7), $S_{c,n}$ can be derived as:

$$S_{c,n} = M_{c,n}\frac{\phi_n(0)\int_0^a r\phi_n(r)dr}{\rho_a} \tag{24}$$

Different from the piston model, the effective force-bearing area $S_{c,n}$ of the centre-mass model is mode dependent and is not equal to the membrane surface area $S = \pi a^2$. Table 1 lists the geometric and material parameters of an example membrane under investigation.

The dimensionless parameter $\lambda_{c,n} = |S_{c,n}/S|$ is defined to indicate the difference between the effective force-bearing area $S_{c,n}$ of the centre-mass model for the nth mode and the membrane surface area $S = \pi a^2$. For the membrane with the parameters listed in Table 1, Table 2 lists $\lambda_{c,n}$ for different modes. It can be noted that for the centre-mass model, mistaking $S = \pi a^2$ for the effective force-bearing area $S_{c,n}$ would cause a fatal error.

2.3. Finite element verification

To verify the proposed SDOF piston model and SDOF centre-mass model for representing the response of the membrane around a certain mode, the commercial software COMSOL Multiphysics is utilized to develop the corresponding finite element model for comparison. COMSOL Multiphysics provides a special module for performing membrane simulation. The developed membrane model in COMSOL Multiphysics is shown in Fig. 3. The displacement of the outer edge of the membrane is completely constrained. The membrane tension is implemented by applying an initial in-plane pre-stress.

For the membrane with the given parameters listed in Table 1, Fig. 4 compares the displacement responses at the membrane centre from COMSOL, the piston model and the centre-mass model. It is worth mentioning that for the piston model, the solution derived from Eq. (22), i.e, $y_n(t)$ corresponds to the space-averaged deflection of the membrane. To make $y_n(t)$ comparable with the results from COMSOL and centre-mass model, it is necessary to use Eq. (16) to convert the space-averaged deflection to the membrane centre displacement.

It can be seen from Fig. 4(a), the result from COMSOL matches well with the results from the piston model and the centre-mass model with the proper use of the derived effective force-bearing area $S_{c,1}$. The fundamental natural frequencies of the COMSOL and piston/centre-mass models are 48.45 and 48.30 Hz, respectively. The maximum displacement amplitudes pre-

Table 1
Geometric and material parameters of the membrane under investigation.

Parameters	Values
Membrane radius a	100 mm
Membrane density ρ	7850 kg/m^3
Membrane thickness h	0.4 mm
Membrane areal density $\rho_a = \rho h$	3.14 kg/m^2
Membrane tension T_s	500 N/m
Damping ratio ζ_n	0.005

Table 2
$\lambda_{c,n}$ for different modes.

Order of mode	$\lambda_{c,n} = \lvert S_{c,n}/S \rvert$
1st mode	0.432
2nd mode	0.123
3rd mode	0.063
4th mode	0.040

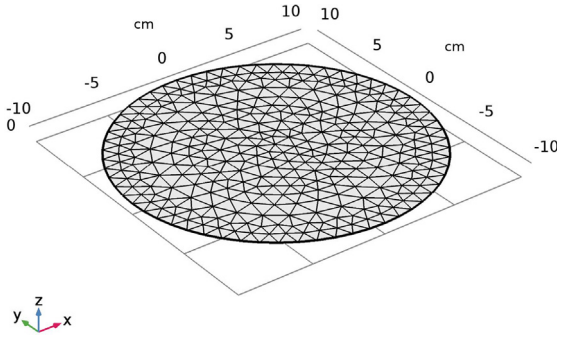

Fig. 3. Finite element model of the membrane in COMSOL Multiphysics.

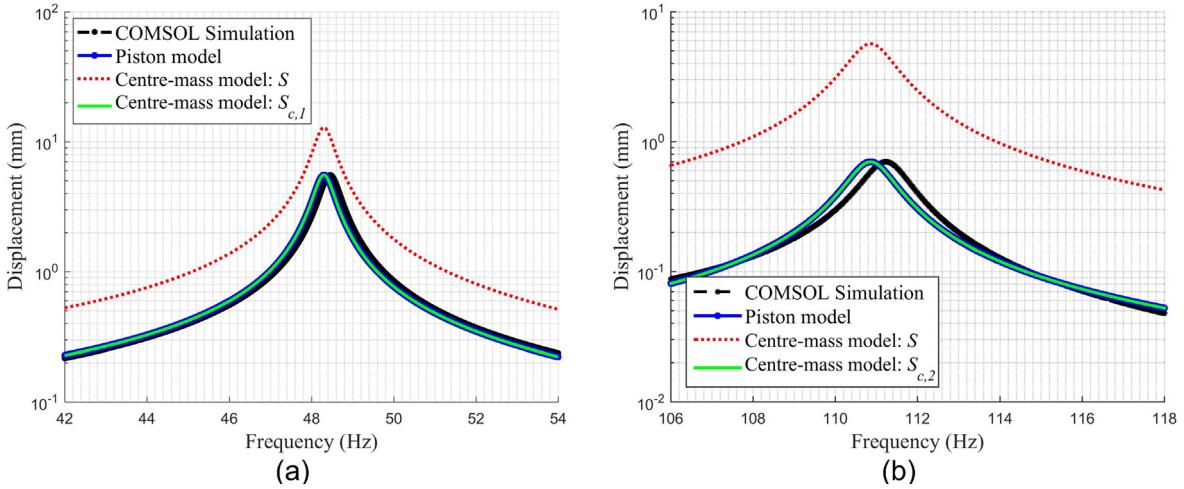

Fig. 4. Comparison of the displacement responses at the membrane centre from COMSOL and the piston/centre-mass models around the (a) fundamental natural frequency; (b) second natural frequency.

dicted by the COMSOL and piston/centre-mass models are 5.5367 and 5.5395 mm, respectively. However, for the centre-mass model, if S is mistaken for its effective force-bearing area in the calculation, a fatal error is produced in the result: the maximum displacement amplitude is 12.8318 mm which is much larger than the authentic value 5.5367 mm due to the overestimation of the effective force-bearing area.

Around the second natural frequency (Fig. 4(b)), it can be observed that the predictions from the piston and centre-mass models are still in a good agreement with COMSOL simulation result. The second natural frequencies of the COMSOL and piston/centre-mass models are 111.24 and 110.86 Hz, respectively. The peak amplitudes from the COMSOL and piston/centre-mass models are 0.6989 and 0.6990 mm, respectively. For the same reason, if S is mistaken for effective force-bearing area rather than $S_{c,2}$, a fatal error occurs in the prediction: the peak amplitude is 5.6690 mm which significantly deviates from 0.6989 mm. Though only the responses near the fundamental and second natural frequencies are presented, it should be mentioned that both the piston and centre-mass models could predict the dynamic behaviours of the membrane for higher modes. It is also worth noting that the proposed models are valid only for predicting the axisymmetric motion of the membrane.

3. MDOF representation of membrane-coupled Helmholtz resonator

As it is well known that, in the low frequency regime, when the wavelength is much larger than the dimension of the Helmholtz resonator, the Helmholtz resonator (Fig. 5(a)) can be modelled as a SDOF oscillating system. The equation of motion of the equivalent SDOF model can be written as:

$$M_1\dot{U}_1 + R_1U_1 + K_1\int U_1 dt = P_1 e^{j\omega t} \tag{25}$$

where $M_1 = \rho_{air}h_{neck}/S_{neck}$ is the equivalent mass. In consideration of the radiation effects at the two ends of the neck, the equivalent mass should be corrected as $M_1 = \rho_{air}(h_{neck} + 1.7r_{neck})/S_{neck}$ [14]. $K_1 = (\rho_{air}c_{air}^2)/V$ is the equivalent stiffness, V is the volume of the cavity, P_1 is the incident pressure. U_1 is the volume flow velocity in the neck. R_1 is the equivalent damping coefficient. Since the bulk viscosity of air is very small [29], R_1 is assumed to be very small and ignored in the following case studies.

3.1. Acoustic-mechanical interaction

In this work, a Helmholtz resonator with the bottom surface being considered as a membrane (as shown in Fig. 5(b)) is studied. When the study involves both acoustic and mechanical systems, it is necessary to consider their interaction (coupling) effects. The principle of developing the model incorporating the interaction is by unifying different physical quantities at the interaction interface based on the analogies between the acoustic and mechanical domains, which are briefly reviewed in Table 3. The analogies to electrical quantities are also presented for later use to develop the equivalent circuit model of the coupled acoustic-mechanical system.

3.1.1. Piston model

At the interface between the membrane and the acoustic field, if we simplified the membrane to a SDOF piston model around nth mode and consider the definition of the mechanical impedance of the membrane and expressing the mechanical quantities by acoustic quantities, the mechanical impedance $Z_{Mechanical}$ and the acoustic impedance $Z_{Acoustic}$ can be related by:

$$Z_{Mechanical} = \frac{F_n}{\langle v_n\rangle} = \frac{P_1 S}{U_n/S} = S^2\frac{P_1}{U_n} = \underbrace{S^2}_{N_{p,n}} Z_{Acoustic} \tag{26}$$

where F_n is the force applied on the piston. As mentioned in Section 2.2, the equivalent force-bearing area in the piston model is exactly S, thus $F_n = P_1 S$. $\langle v_n\rangle$ is the mechanical flow quantity, i.e., the velocity of the piston (the space-averaged velocity of the membrane). Therefore, the mechanical-acoustic transformation coefficient is

$$N_{p,n} = S^2 \tag{27}$$

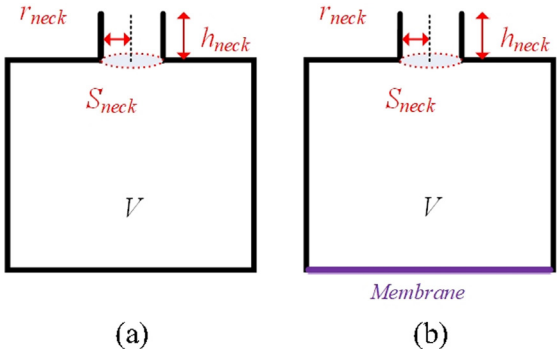

Fig. 5. (a) Schematic of a Helmholtz resonator; (b) schematic of a membrane-coupled Helmholtz resonator.

Table 3
Electro-Acoustic-Mechanical analogies.

	Potential quantity	Flow quantity
Electrical system	Voltage	Current
Mechanical system	Force	Velocity
Acoustic system	Sound pressure	Volume velocity

which is actually the same as that for an exact piston, regardless of the order of mode.

3.1.2. Centre-mass model

Following the same procedure, we can obtain the mechanical-acoustic transformation relation could be obtained for the centre-mass model:

$$Z_{Mechanical} = \frac{F_n}{v_n} = \frac{P_1 S_{c,n}}{\langle v_n \rangle / \beta_n} = \frac{P_1 S_{c,n}}{(U_n/S)/\beta_n} = \beta_n S S_{c,n} \frac{P_1}{U_n} = \underbrace{\beta_n S S_{c,n}}_{N_{c,n}} Z_{Acoustic} \tag{28}$$

where F_n is the force applied on the centre mass. Because the equivalent force-bearing area $S_{c,n}$ depends on modes, $F_n = P_1 S_{c,n}$ is different if we simplified the membrane to a SDOF model in different modes. v_n is the mechanical flow quantity, i.e., the velocity of the centre mass (the velocity of the membrane centre). The mechanical-acoustic transformation coefficient for the centre-mass model is

$$N_{c,n} = \beta_n S S_{c,n} \tag{29}$$

It can be noted that an additional parameter β_n (which has been defined in Eq. (16)) appears in the mechanical-acoustic transformation relation equation for the centre-mass model. This is because the centre-mass model assumes that all the equivalent parameters are concentrated at the membrane centre. When we convert the mechanical flow quantity v_n into the acoustic flow quantity U_n, the centre velocity v_n needs to be converted into the space-averaged velocity $\langle v_n \rangle$ first with the help of Eq. (16).

3.2. MDOF model

The mechanical quantities of the membrane have already been converted into equivalent acoustic quantities by using the derived mechanical-acoustic transformation coefficients (Eqs. (27) and (29)). The equivalent lumped parameters of the Helmholtz resonator (which are presented in Eq. (25)) are given out by numerous existing literature. It can be expected that the coupling of the Helmholtz resonator and the membrane will constitute a MDOF system. We can either use piston model or centre-mass model to represent the membrane and it turns out to give the same results, which will be proved in the following study.

By using the electro-acoustic-mechanical analogies and considering the volume flow balance at the acoustic-mechanical interaction interface (an analogy to Kirchhoff's current law), the equivalent circuit model of the membrane-coupled Helmholtz resonator can be developed as shown in Fig. 6(a). The corresponding equivalent mechanical model of the membrane-coupled Helmholtz resonator is shown in Fig. 6(b). The governing equation of this acoustic-mechanical system can be written as:

$$\begin{cases} M_1 \dot{U}_1 + K_1 \int (U_1 - U_2) dt = P_1 e^{j\omega t} \\ M_2 \dot{U}_2 + D_2 U_2 + K_2 \int U_2 dt + K_1 \int (U_2 - U_1) dt = 0 \end{cases} \tag{30}$$

where $M_2 = M_{p,1}/N_{p,1} = M_{c,1}/N_{c,1}$, $K_2 = K_{p,1}/N_{p,1} = K_{c,1}/N_{c,1}$, $D_2 = D_{p,1}/N_{p,1} = D_{c,1}/N_{c,1}$, U_1 is the volume velocity of the air in the neck of the Helmholtz resonator, U_2 is the volume velocity of the air aroused by the membrane first mode vibration. In this model, the Helmholtz resonator and the membrane are treated and represented by two DOFs, then coupled to form a 2DOF system. It is expected to predict the dynamic behaviour of the coupled system around its first two natural frequencies by using Eq. (30). However, since the natural frequencies of the first two modes of the membrane are not separated far away,

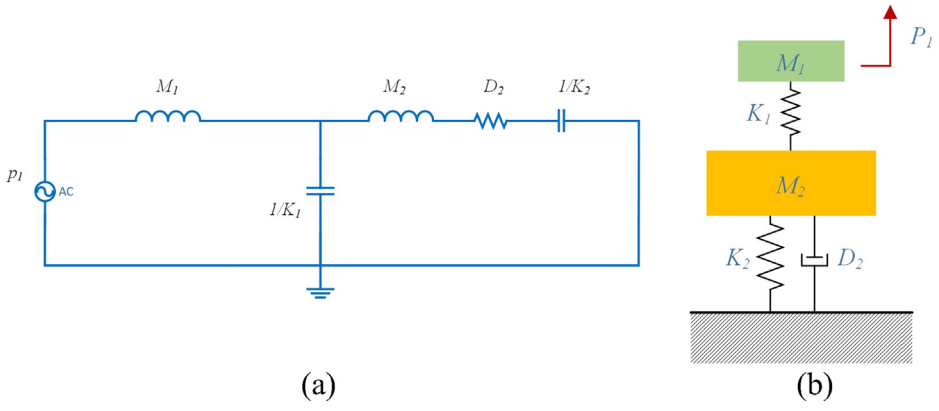

Fig. 6. (a) Equivalent circuit model and (b) equivalent mechanical model of the membrane-coupled Helmholtz resonator (2DOF model considering only the first mode of the membrane).

based on the principle of the modal superposition, it can be speculated that the modal contribution from the second mode of the membrane will be not negligible as compared to that from the first mode in the response. For this reason, to improve the accuracy, it is necessary to include more modes into consideration. Starting from the modal equation, i.e, Eq. (4), and recalling that the actual response should be the superposition of all the modal responses, i.e., Eq. (7), it is not difficult to obtain the following governing equation by including the second mode of the membrane.

$$\begin{cases} M_1\dot{U}_1 + K_1\int(U_1 - U_2 - U_3)dt = P_1 e^{j\omega t} \\ M_2\dot{U}_2 + D_2U_2 + K_2\int U_2 dt + K_1\int(U_2 + U_3 - U_1)dt = 0 \\ M_3\dot{U}_3 + D_3U_3 + K_3\int U_3 dt + K_1\int(U_2 + U_3 - U_1)dt = 0 \end{cases} \tag{31}$$

where $M_3 = M_{p,2}/N_{p,2} = M_{c,2}/N_{c,2}$,$K_3 = K_{p,2}/N_{p,2} = K_{c,2}/N_{c,2}$,$D_3 = D_{p,2}/N_{p,2} = D_{c,2}/N_{c,2}$, U_3 is the volume velocity of the air aroused by the membrane second mode vibration. The corresponding equivalent circuit of Eq. (31) is presented in Fig. 7. It can be seen that by including the second mode of the membrane into account, the coupled system has three DOFs.

3.3. Finite element verification

Finite element analysis is performed using COMSOL Multiphysics to verify the MDOF models of the membrane-coupled Helmholtz resonator. The developed finite element model is shown in Fig. 8 with the parameters listed in Table 4. The bottom surface of the Helmholtz resonator is the membrane with the same parameters listed in Table 1.

Fig. 9 presents the predicted centre displacement responses of the membrane of membrane-coupled Helmholtz resonator from COMSOL and MDOF models. The first two natural frequencies calculated by COMSOL are 33.549 and 83.569 Hz, respectively, and the corresponding amplitudes of the first two peaks are 10.950 and 3.541 mm, respectively. From Fig. 9(a), it can be found that when only the fundamental mode is used (i.e., Eq. (30)), the prediction by the piston model around the first peak matches with the result from COMSOL: the fundamental natural frequency is 34.046 Hz and the amplitude of the first peak is 11.37 mm. However, the prediction around the 2nd mode has an obvious deviation: the second natural frequency is 86.894 Hz and the amplitude of the second peak is 3.040 mm. When the first two modes are taken into account (i.e., Eq. (31)),

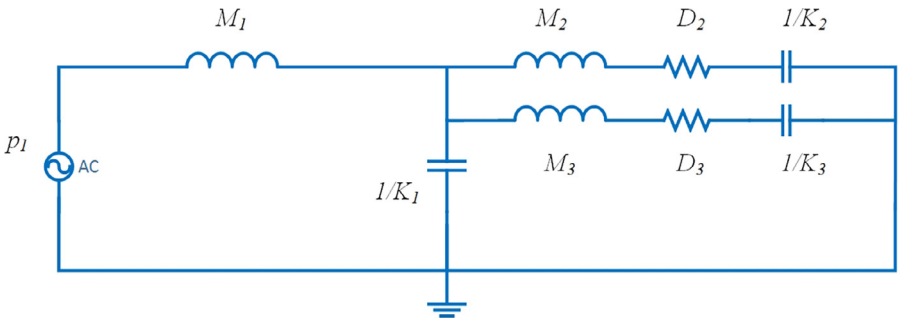

Fig. 7. Equivalent circuit model of the membrane-coupled Helmholtz resonator (3DOF model considering the first two modes of the membrane).

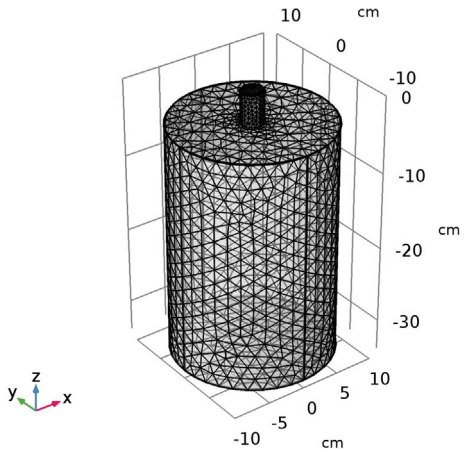

Fig. 8. Finite element model of the membrane-coupled Helmholtz resonator in COMSOL Multiphysics.

Table 4
Parameters of the Helmholtz resonator.

Parameter	Value
Radius of the neck r_{neck}	1.4 cm
Radius of the cavity r_{cavity}	10 cm
Length of the neck h_{neck}	4 cm
Length of the cavity h_{cavity}	30 cm
Density of air ρ_{air}	1.2 kg/m^3
Sound speed c_{air}	343 m/s

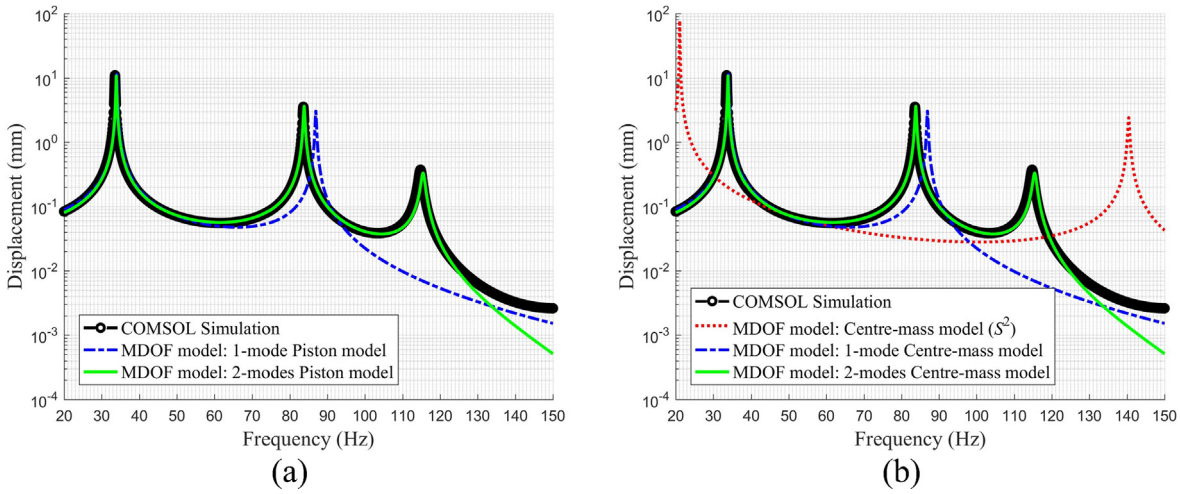

Fig. 9. Membrane centre displacement responses from COMSOL and developed MDOF models of membrane-coupled Helmholtz resonator: (a) membrane represented by piston model; (b) membrane represented by centre-mass model.

the second peak shows a better agreement with the result from COMSOL: the second natural frequency is 83.784 Hz and the amplitude of the second peak is 3.605 mm, which is more consistent with the results from COMSOL. Moreover, the accuracy of the prediction in terms of the first peak is also improved: the fundamental natural frequency is 33.906 Hz and the amplitude of the first peak is 10.730 mm. The results of the centre-mass model (Fig. 9(b)) is exactly the same as those of the piston model (Fig. 9(a)). However, it is noteworthy that if the acoustic-mechanical transformation coefficient $N_{c,1}$ of the centre-mass model is mistaken by using S^2, there could result in significant error in the prediction in terms of the first two natural frequencies and the amplitudes of the first two peaks of the coupled system.

3.4. Further discussion

It is well known that the natural frequencies of a coupled system deviate from the natural frequencies of the independent systems that constitute the coupled system [30]. If the natural frequencies of the membrane-coupled Helmholtz resonator deviate from the fundamental natural frequency of the membrane, but are still at the same order of the fundamental natural frequency and much smaller than the second natural frequency of the Helmholtz resonator, one can include more axisymmetric modes of the membrane into consideration for improving the modelling accuracy. However, if the natural frequencies of the membrane-coupled Helmholtz resonator deviate far away from the fundamental natural frequency of the Helmholtz resonator, the proposed MDOF representation modelling method becomes invalid for predicting the dynamic behaviour of the membrane-coupled Helmholtz resonator. Since the current method adopts the theory of simplifying the Helmholtz resonator as an SDOF system, higher-order mode vibrations of the Helmholtz resonator are essentially ignored. In summary, it should be emphasized that the proposed MDOF representation method is only valid when the natural frequencies of the membrane-coupled Helmholtz resonator are still of the same order of the fundamental natural frequency of the Helmholtz resonator.

4. Acoustic metamaterial using membrane-coupled Helmholtz resonator

From the above study, it is noted that the membrane-coupled Helmholtz resonator generates multiple resonances in the low frequency regime. Xiao et al. [31] proposed a metamaterial rod containing MDOF local resonators and achieved multiple band gaps for forbidding longitudinal elastic wave propagation. Since the nature of sound is also a longitudinal wave and the

sound wave equation has exactly the same mathematical form as the wave equation for longitudinal waves in a rod, it is motivated to implement the MDOF membrane-coupled Helmholtz resonator in the design of an acoustic metamaterial for achieving multiple band gaps. To distinguish the MDOF models of the membrane-coupled Helmholtz resonator (MCHR) incorporating one mode or two modes of the membrane, they are referred to as 1-mode MDOF MCHR and 2-mode MDOF MCHR, respectively.

4.1. Theoretical model

Fig. 10 shows the schematic of the proposed acoustic metamaterial system. The membrane-coupled Helmholtz resonators are periodically arranged along a main duct at a constant spacing of d. The cross-section area of the main duct is S_0. The wave equation of the sound pressure p propagating in the main duct can be expressed as:

$$\frac{\partial^2 p}{\partial x^2} = \frac{1}{c_{air}^2}\frac{\partial^2 p}{\partial t^2} \tag{32}$$

Only the steady-state harmonic response is of interest. The time factor that applies to all the field variables can thus be disregarded. The general solution of the pressure amplitude in the nth unit cell is assumed to be:

$$P_n(x_n) = A_n\cos(\alpha x_n) + B_n\sin(\alpha x_n) \tag{33}$$

where $\alpha = \omega/c_{air}$. The wave speed is given by:

$$V_n(x_n) = \frac{A_n}{j\rho_{air}c_{air}}\sin(\alpha x_n) - \frac{B_n}{j\rho_{air}c_{air}}\cos(\alpha x_n) \tag{34}$$

At the intersection between the nth and $(n+1)$th unit cells, the continuity condition yields:

$$\begin{cases} P_n|_{x_n=d} = P_{n+1}|_{x_{n+1}=0} \\ U_n|_{x_n=d} - U_{n+1}|_{x_{n+1}=0} = \frac{P_{n+1}|_{x_{n+1}=0}}{Z_{n+1}} \end{cases} \tag{35}$$

where Z_{n+1} is the acoustic impedance of the $(n+1)$th membrane-coupled Helmholtz resonator, $U_n = V_n S_0$ and $U_{n+1} = V_{n+1}S_0$ are the volume velocities in the nth and $(n+1)$th unit cells, respectively. If the membrane-coupled Helmholtz resonator is represented by the 1-mode MDOF model (Fig. 6(a)), then

$$Z_{n+1} = \left\{ j\left(\omega M_2 - \frac{K_2}{\omega}\right) \| \left(-j\frac{K_1}{\omega}\right) \right\} + j\omega M_1 \tag{36}$$

If the membraned coupled Helmholtz resonator is represented by the 2-mode MDOF model (Fig. 7), then

$$Z_{n+1} = \left\{ \left[j\left(\omega M_2 - \frac{K_2}{\omega}\right) \| j\left(\omega M_3 - \frac{K_3}{\omega}\right) \right] \| \left(-j\frac{K_1}{\omega}\right) \right\} + j\omega M_1 \tag{37}$$

By substituting Eqs. (33) and (34) into Eq. (35), the transfer matrix that relates the nth and $(n+1)$th unit cells can be obtained:

$$\begin{bmatrix} A_{n+1} \\ B_{n+1} \end{bmatrix} = \mathbf{T}\begin{bmatrix} A_n \\ B_n \end{bmatrix} \tag{38}$$

where $\mathbf{T} = \mathbf{H}^{-1}\mathbf{K}$, $\mathbf{K} = \begin{bmatrix} \cos(\alpha d) & \sin(\alpha d) \\ \sin(\alpha d) & -\cos(\alpha d) \end{bmatrix}$ and $\mathbf{H} = \begin{bmatrix} 1 & 0 \\ \chi & -1 \end{bmatrix}$, $\chi = \frac{\rho_{air}c_{air}}{-jS_0 Z_{n+1}}$. On the other hand, by using the Bloch's theorem, the periodicity condition yields:

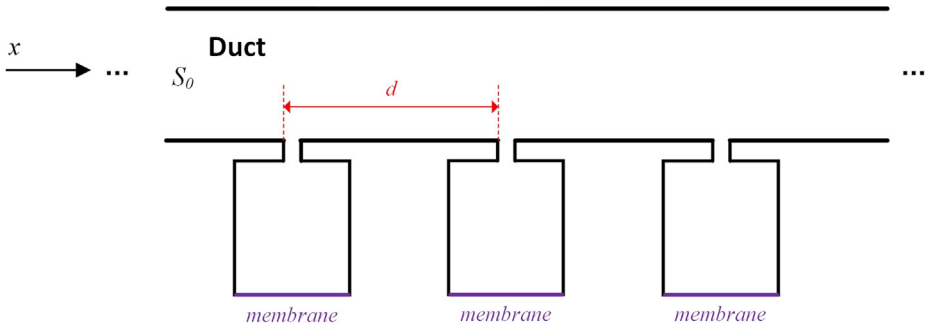

Fig. 10. Schematic of acoustic metamaterial using membrane-coupled Helmholtz resonators.

$$\begin{bmatrix} A_{n+1} \\ B_{n+1} \end{bmatrix} = e^{iqd} \begin{bmatrix} A_n \\ B_n \end{bmatrix} \tag{39}$$

where q is the wavenumber. Therefore, a standard eigenvalue problem is obtained:

$$\left|\mathbf{T} - e^{iqd}\mathbf{I}\right| = 0 \tag{40}$$

By sweeping ω and simultaneously seeking the solution to q based on Eq. (40), one obtains the dispersion relation of the proposed acoustic metamaterial system.

4.2. Finite element verification

Finite element analysis is performed using COMSOL Multiphysics to verify the developed model for the acoustic metamaterial system. The parameters of the membrane-coupled Helmholtz resonator are the same as those used in the previous case studies (Tables 1 and 4). With $S_0 = 10$ cm $\times$ 20 cm and $d = 100$ cm, the finite element model is developed, as shown in Fig. 11.

Fig. 12 compares the band structures of the proposed acoustic metamaterial system calculated by COMSOL and the developed theoretical model. For the theoretical results presented in Fig. 12(a) and (b), the membrane-coupled Helmholtz resonator are represented by the 1-mode and 2-modes MDOF models, respectively. The detailed band gap ranges from COMSOL and theoretical models are listed in Table 5. It can be found that in terms of the first band gap in the low frequency

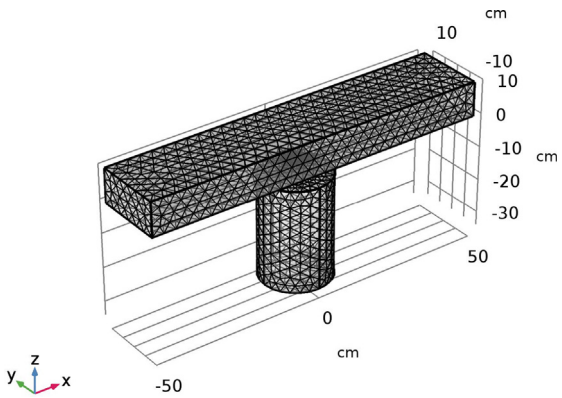

Fig. 11. Finite element model of the acoustic metamaterial system in COMSOL Multiphysics.

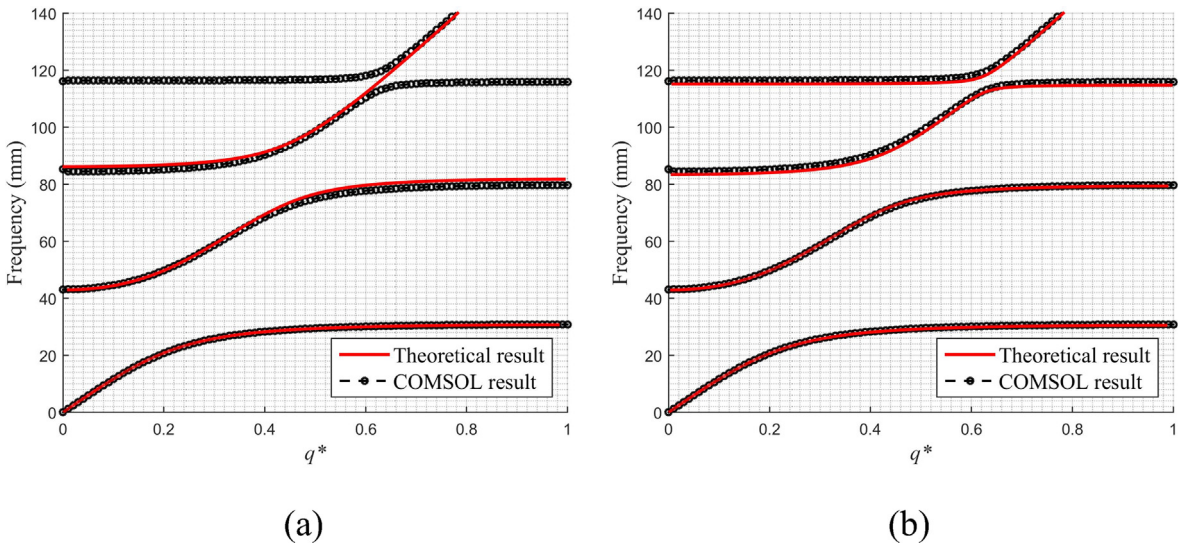

Fig. 12. Band structures calculated by COMSOL and theoretical model with the membrane-coupled Helmholtz resonator described by: (a) 1-mode MDOF MCHR model; (b) 2-mode MDOF MCHR model. Note that $q^* = q/\pi$ is the dimensionless wave number.

Table 5
Band gap ranges predicted by COMSOL and theoretical models.

Band gap	Acoustic Metamaterial Model	Lower bound	Upper bound
1st band gap	COMSOL model	30.79 Hz	43.02 Hz
	Theoretical model with 1-mode MDOF MCHR	30.67 Hz	42.94 Hz
	Theoretical model with 2-mode MDOFMCHR	30.51 Hz	42.91 Hz
2nd band gap	COMSOL model	79.73 Hz	85.33 Hz
	Theoretical model with 1-mode MDOF MCHR	81.77 Hz	86.17 Hz
	Theoretical model with 2-mode MDOF MCHR	79.39 Hz	83.40 Hz
3rd band gap	COMSOL model	115.90 Hz	116.2 Hz
	Theoretical model with 1-mode MDOF MCHR	N.A.	N.A.
	Theoretical model with 2-modes MDOF MCHR	114.80 Hz	115.20 Hz

regime, the theoretical model using 1-mode or 2-mode MDOF MCHR models gives good prediction as compared to the results from COMSOL. The model with 2-mode MDOF MCHR gives better prediction for the second band gap. In addition, it is worth noting that for the theoretical result with 2-mode MDOF MCHR, because one more mode of the membrane is taken into account, the third band gap can be predicted by the theoretical model (Fig. 12(b)), though a bit larger deviation exists as compared to the result from COMSOL (Table 5). It can be speculated that by including more modes into consideration, the prediction accuracy can be further improved and more band gaps could possibly be predicted. However, it is important to note that the Helmholtz resonator itself is only treated as a SDOF. This treatment only validates in the low frequency regime. Therefore, this theoretical method is only applicable for low frequency regime analysis.

5. Conclusions

This paper presents a theoretical study on the modelling of the membrane, the membrane-coupled Helmholtz resonator with lumped parameters, and the acoustic metamaterial system integrated with the membrane-coupled Helmholtz resonators. Two SDOF models, i.e., piston model and centre-mass model, have been developed for predicting the dynamic behaviour of the membrane. The equivalent lumped parameters are derived and the difference in the effective force-bearing area between the two models has been discussed. The piston and centre-mass models have been verified by the finite element model. On the basis of the SDOF representation of the membrane, the membrane-coupled Helmholtz resonator is modelled as a MDOF system. Transformation coefficients are introduced to consider the acoustic-mechanical interaction, thus bridging the acoustic and mechanical domains. Finite element verification of the proposed MDOF models for describing the membrane-coupled Helmholtz resonator has been provided. A novel acoustic metamaterial system integrated with the membrane-coupled Helmholtz resonators is then proposed. The band structure analysis based on theoretical model and finite element model shows that the proposed acoustic metamaterial system can produce multiple band gaps in the low frequency regime. The models incorporating 2 modes of the membranes could improve the prediction in the dynamic response of the membrane-coupled Helmholtz resonator and the band gap of the acoustic metamaterial system.

Acknowledgments

This work is financially supported by the PhD scholarship from China Scholarship Council (no. 201608250001) and Jiangsu Overseas Visiting Scholar Program for University Prominent Young & Middle-aged Teachers and Presidents (JDPE).

References

[1] P. Tang, W. Sirignano, Theory of a generalized Helmholtz resonator, J. Sound Vib. 26 (2) (1973) 247–262.
[2] L. Rayleigh, The theory of the Helmholtz resonator, Proc. Royal Soc. London, Ser. A 92 (638) (1916) 265–275.
[3] S.B. Horowitz, M. Sheplak, L.N. Cattafesta III, T. Nishida, A MEMS acoustic energy harvester, J. Micromech. Microeng. 16 (9) (2006) S174.
[4] A. Yang, P. Li, Y. Wen, C. Lu, X. Peng, W. He, J. Zhang, D. Wang, F. Yang, Note: High-efficiency broadband acoustic energy harvesting using Helmholtz resonator and dual piezoelectric cantilever beams, Rev. Sci. Instrum. 85 (6) (2014) 066103.
[5] A.B. Atrah, H. Salleh, Simulation of acoustic energy harvester using helmholtz resonator with piezoelectric backplate, Proceedings of the 20th International Congress on Sound and Vibration (ICSV20), Bangkok, Thailand, July, 2013.
[6] G.-S. Liu, Y.-Y. Peng, M.-H. Liu, X.-Y. Zou, J.-C. Cheng, Broadband acoustic energy harvesting metasurface with coupled Helmholtz resonators, Appl. Phys. Lett. 113 (15) (2018) 153503.
[7] N. Fang, D. Xi, J. Xu, M. Ambati, W. Srituravanich, C. Sun, X. Zhang, Ultrasonic metamaterials with negative modulus, Nat. Mater. 5 (6) (2006) 452.
[8] J. Li, W. Wang, Y. Xie, B.-I. Popa, S.A. Cummer, A sound absorbing metasurface with coupled resonators, Appl. Phys. Lett. 109 (9) (2016) 091908.
[9] Z.G. Wang, S.H. Lee, C.K. Kim, C.M. Park, K. Nahm, S. Nikitov, Acoustic wave propagation in one-dimensional phononic crystals containing Helmholtz resonators, J. Appl. Phys. 103 (6) (2008) 064907.
[10] S.-H. Seo, Y.-H. Kim, Silencer design by using array resonators for low-frequency band noise reduction, J. Acoustical Soc. Am. 118 (4) (2005) 2332–2338.
[11] O. Richoux, V. Pagneux, Acoustic characterization of the Hofstadter butterfly with resonant scatterers, EPL (Europhysics Letters). 59 (1) (2002) 34.
[12] F. Liu, S. Horowitz, T. Nishida, L. Cattafesta, M. Sheplak, A multiple degree of freedom electromechanical Helmholtz resonator, J. Acoustical Soc. Am. 122 (1) (2007) 291–301.

[13] F. Liu, A. Phipps, S. Horowitz, K. Ngo, L. Cattafesta, T. Nishida, M. Sheplak, Acoustic energy harvesting using an electromechanical Helmholtz resonator, J. Acoustical Soc. Am. 123 (4) (2008) 1983–1990.
[14] S. Matova, R. Elfrink, R. Vullers, R. Van Schaijk, Harvesting energy from airflow with a michromachined piezoelectric harvester inside a Helmholtz resonator, J. Micromech. Microeng. 21 (10) (2011) 104001.
[15] X. Peng, Y. Wen, P. Li, A. Yang, X. Bai, A wideband acoustic energy harvester using a three degree-of-freedom architecture, Appl. Phys. Lett. 103 (16) (2013) 164106.
[16] S. Shi, T. New, Y. Liu, Flapping dynamics of a low aspect-ratio energy-harvesting membrane immersed in a square cylinder wake, Exp. Therm Fluid Sci. 46 (2013) 151–161.
[17] H. Nguyen, R. Zhu, J. Chen, S. Tracy, G. Huang, Analytical coupled modeling of a magneto-based acoustic metamaterial harvester, Smart Mater. Struct. 27 (5) (2018) 055010.
[18] A. Yang, P. Li, Y. Wen, C. Lu, X. Peng, J. Zhang, W. He, Enhanced acoustic energy harvesting using coupled resonance structure of sonic crystal and Helmholtz resonator, Appl. Phys Express 6 (12) (2013) 127101.
[19] S. Noh, H. Lee, B. Choi, A study on the acoustic energy harvesting with Helmholtz resonator and piezoelectric cantilevers, Int. J. Precis. Eng. Manuf. 14 (9) (2013) 1629–1635.
[20] Z. Yang, J. Mei, M. Yang, N. Chan, P. Sheng, Membrane-type acoustic metamaterial with negative dynamic mass, Phys. Rev. Lett. 101 (20) (2008) 204301.
[21] G. Ma, M. Yang, S. Xiao, Z. Yang, P. Sheng, Acoustic metasurface with hybrid resonances, Nat. Mater. 13 (9) (2014) 873.
[22] M. Yang, G. Ma, Z. Yang, P. Sheng, Coupled membranes with doubly negative mass density and bulk modulus, Phys. Rev. Lett. 110 (13) (2013) 134301.
[23] J. Li, X. Zhou, G. Huang, G. Hu, Acoustic metamaterials capable of both sound insulation and energy harvesting, Smart Mater. Struct. 25 (4) (2016) 045013.
[24] N. Gao, J. Wu, H. Hou, L. Yu, Excellent low-frequency sound absorption of radial membrane acoustic metamaterial, Int. J. Mod Phys B 31 (3) (2017) 1750011.
[25] A. Abbad, K. Rabenorosoa, M. Ouisse, N. Atalla, Adaptive Helmholtz resonator based on electroactive polymers: modeling, characterization, and control, Smart Mater. Struct. 27 (10) (2018) 105029.
[26] X. Zhu, Z. Chen, Y. Jiao, Y. Wang, Broadening of the sound absorption bandwidth of the perforated panel using a membrane-type resonator, J. Vib. Acoust. 140 (3) (2018) 031014.
[27] A. Abbad, Numerical investigations on a tunable helmholtz resonator: integration of a passive polymer membrane in a helmholtz resonator, SAE Technical Paper, 2016.
[28] P.M. Morse, A.S.O. America, A.I.O. Physics, Vibration and Sound, McGraw-Hill, New York, 1948.
[29] E.W. Lemmon, R. Jacobsen, Viscosity and thermal conductivity equations for nitrogen, oxygen, argon, and air, Int. J. Thermophys. 25 (1) (2004) 21–69.
[30] S.S. Rao, F.F. Yap, Mechanical Vibrations, Prentice hall, Upper Saddle River, 2011.
[31] Y. Xiao, J. Wen, X. Wen, Longitudinal wave band gaps in metamaterial-based elastic rods containing multi-degree-of-freedom resonators, New J. Phys. 14 (3) (2012) 033042.